ACS Energy LETTERS

http://pubs.acs.org/journal/aelccp

Thin and Flexible Solid Electrolyte Membranes with Ultrahigh Thermal Stability Derived from Solution-Processable Li Argyrodites for All-Solid-State Li-Ion Batteries

Dong Hyeon Kim,[⊥] Yong-Hyeok Lee,[⊥] Yong Bae Song, Hiram Kwak, Sang-Young Lee,* and Yoon Seok Jung*

Cite This: *ACS Energy Lett.* 2020, 5, 718−727

Read Online

ACCESS | Metrics & More | Article Recommendations | Supporting Information

ABSTRACT: Sheet-type solid electrolyte (SE) membranes are essential for practical all-solid-state Li batteries (ASLBs). To date, SE membrane development has mostly been based on polymer electrolytes with or without the aid of liquid electrolytes, which offset thermal stability (or safety). In this study, a new scalable fabrication protocol for thin (40−70 μm) and flexible single-ion conducting sulfide SE membranes with high conductance (29 mS) and excellent thermal stability (up to ∼400 °C) is reported. Electrospun polyimide (PI) nonwovens provide a favorable porous structure and ultrahigh thermal stability, thus accommodating highly conductive infiltrating solution-processable $Li_6PS_5Cl_{0.5}Br_{0.5}$ (2.0 mS cm^{-1}). $LiNi_{0.6}Co_{0.2}Mn_{0.2}O_2$/graphite ASLBs using 40 μm thick $Li_6PS_5Cl_{0.5}Br_{0.5}$-infiltrated PI membranes show promising performances at 30 °C (146 mA h g^{-1}) and excellent thermal stability (marginal degradation at 180 °C). Moreover, a new proof-of-concept fabrication protocol for ASLBs at scale that involves the injection of liquefied SEs into the electrode/PI/electrode assemblies is successfully demonstrated for $LiCoO_2$/PI−$Li_6PS_5Cl_{0.5}Br_{0.5}$/$Li_4Ti_5O_{12}$ ASLBs.

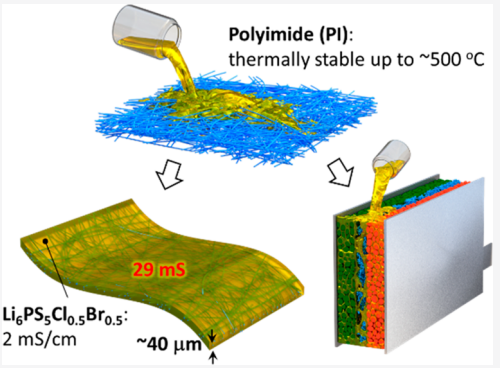

For the past 20 years, lithium-ion batteries (LIBs) have dominated the market for portable electronic devices due to their high energy and power densities. The development of liquid electrolytes (LEs) based on $LiPF_6$ in carbonate-based organic solvents has enabled the stabilization of high-voltage electrode chemistries for commercial LIBs.[1−3] However, the flammability of organic LEs threatens the success of LIBs in the next stage for large-scale applications such as battery-driven electric vehicles and energy storage systems.[4−6] Accordingly, solidification of electrolytes using inorganic solid electrolyte (SE) materials to achieve all-solid-state batteries is considered one of the most reasonable directions for future progress.[7−13] Several sulfide superionic conductors have reached extremely high conductivities of >10^{-2} S cm^{-1} at room temperature (e.g., $Li_{9.54}Si_{1.74}P_{1.44}S_{11.7}Cl_{0.3}$, 2.5 × 10^{-2} S cm^{-1}; $Li_{5.5}PS_{4.5}Cl_{1.5}$, 9.4 × 10^{-3} S cm^{-1}). These are comparable to those for LEs.[10,14−17] In addition, sulfide SE materials are relatively light [e.g., 1.86 g cm^{-3} for Li_6PS_5Cl vs 5.01 g cm^{-3} for $Li_7La_3Zr_2O_{12}$ and 2.94 g cm^{-3} for $Li_{1.3}Al_{0.3}Ti_{1.7}(PO_4)_3$] and can be deformed mechanically for sintering at room temperature, which makes them a promising candidate for practical all-solid-state Li batteries (ASLBs).[7,11,18,19]

Composite-structured bulk-type ASLBs are promising because they can adopt the wet-slurry process based on powder-type electrode materials, which has already been commercialized for LIB manufacturing.[20−25] To date, several efforts have been devoted to the development of sheet-type electrodes for ASLBs and have shown noticeable progress in terms of capacity and rate capability.[23,24] A common practice is to use ultrathick (typically >500 μm) SE layers between two electrodes to fabricate ASLB test cells.[20,24,25] However, in terms of cell-based energy density for practical large-format ASLBs, SE layers with thicknesses of <100 μm are required.[26,27] In addition, their scalable fabrication is of

Received: February 4, 2020
Accepted: February 7, 2020
Published: February 7, 2020

https://dx.doi.org/10.1021/acsenergylett.0c00251
ACS Energy Lett. 2020, 5, 718−727

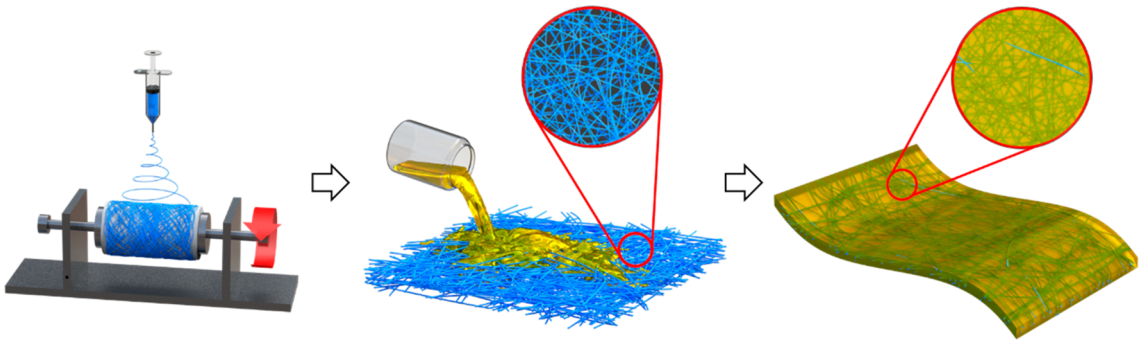

Figure 1. Schematic illustrating the fabrication of sulfide SE membranes for ASLBs by infiltration of electrospun porous PI NWs with solution-processable $Li_6PS_5[Cl,Br]$.

prime importance. An SE layer could be overcoated on as-formed electrode layers using the wet-slurry method.[22,23,28] However, overcasting thin SE layers uniformly in a large area may be hindered by possible intermixing of the SE and electrode layers and by the non-ideal flatness of the as-formed electrode layer surfaces.[27,28] Thus, the development of free-standing and thin SE membranes, which are an ASLB analogue to the separator for conventional LIBs, could be an alternative solution.

To this end, the introduction of a soft polymeric component is required. In most relevant previous works, hybridization between polymer electrolytes and oxide fillers has been developed.[29−37] The incorporation of oxide SEs in a polymer electrolyte matrix could achieve ionic conductivities of $\sim 10^{-4}$ S cm^{-1} at room temperature, which could be explained by the facilitated Li^+ pathways at interfaces.[29,30,35,36] However, the corresponding electrochemical performances have been far from satisfactory. This is reflected in results obtained with cells in which small amounts of LEs were added and/or tested at elevated temperatures (50−80 °C).[29,30,36] Moreover, poly(ethylene oxide) (PEO), which is the most popular polymeric host in these conventional oxide−polymer composite (OPC) SE membranes, suffers from poor electrochemical oxidation stability (<4 V vs Li/Li^+).[29,31,38] Recently, it was reported that the use of multilayered SE membranes consisting of oxidation-stable poly(acrylonitrile) and reduction-resistant polyethylene glycol diacrylate with the aid of a small amount of LEs enabled the operation of $LiNi_{0.8}Co_{0.1}Mn_{0.1}O_2$/Li cells at room temperature.[37] More importantly, polymeric components in conventional OPC SE membranes degrade the thermal stability of SE layers, which offsets the critical advantage of ASLBs and in turn might degrade safety performance. It is thus highly desirable that the SE membranes for ASLBs should maintain their original dimensions at elevated temperatures without suffering failure (i.e., internal short circuit) caused by shrinkage and/or melting.[39,40]

By contrast, despite the favorable properties of sulfide SEs, only a few reports have been conducted on sulfide-based SE membranes. This is because of the complications of the wet-slurry method arising from their poor chemical stability.[22,41,42] In our previous work, bendable and thin SE membranes were fabricated by impregnation of the macroporous polymeric nonwoven (NW) scaffold with sulfide SE particles.[27] Lee and co-workers reported $77.5Li_2S$-$22.5P_2S_5$ in a self-healing polymer matrix.[26] Nazar and co-workers fabricated a Li_3PS_4-based membrane by infiltration with an elastic polymer and assembled $Li_4Ti_5O_{12}$/Li cells.[43] Kobayashi and co-workers reported self-standing sulfide SE sheets fabricated by slurry coating on a copper foil, followed by exfoliation.[21] Xu and co-workers fabricated PEO-based hybrid polymer electrolytes that included 2 vol % Li_3PS_4 as nanosized fillers by in situ preparation.[44]

Previously, our group demonstrated that solution-processable sulfide SEs, including Li_6PS_5Cl using ethanol (EtOH), (LiI-)Li_4SnS_4 using methanol or water, and Na_3SbS_4 using methanol or water, could be applied for direct SE coatings onto electrode active materials, circumventing the poor solid−solid ionic contact problem occurring in all-solid-state electrodes.[45−48] Moreover, infiltration of conventional LIB electrodes with solution-processable SEs could directly lead to obtaining ASLB electrodes, thus bypassing the complications posed by the sulfide-based slurry method.[41,49]

On the basis of this background and these motivations, we report facile and scalable fabrication of thin (40−70 μm thick) sulfide SE membranes with high conductance (29 mS at 30 °C) by infiltration of highly porous electrospun polyimide (PI) NWs with solution-processable Li argyrodites ($Li_6PS_5[Cl,Br]$). The excellent thermal stability of PI enables heat treatment at high temperatures of ≤400 °C, which is necessary to achieve the high conductivity of the solution-processed $Li_6PS_5Cl_{0.5}Br_{0.5}$ of 2 mS cm^{-1} at 30 °C. $LiNi_{0.6}Co_{0.2}Mn_{0.2}O_2$ (NCM)/graphite (Gr) all-solid-state full cells using the 40 μm thick $Li_6PS_5Cl_{0.5}Br_{0.5}$-infiltrated PI membranes show a high reversible capacity and energy density of 146 mA h g_{NCM}^{-1} and 110 W h kg_{cell}^{-1} (including the masses of current collectors), respectively, at 30 °C. In addition, their negligible capacity fading after exposure to a high temperature of 180 °C highlights the exceptionally high thermal stability. Furthermore, inspired by the already-commercialized LE injection process used in LIB manufacturing, the new fabrication protocol for ASLBs that involves the injection of liquefied SEs into preassembled $Al/LiCoO_2$/(PI NW)/$Li_4Ti_5O_{12}$/Al and solidification is demonstrated for the first time.

The fabrication procedure for SE membranes by the infiltration of solution-processable $Li_6PS_5[Cl,Br]$ into electrospun porous PI NW scaffolds is illustrated in Figure 1. Critical factors in the design strategy for polymeric NW scaffolds are (i) good mechanical strength, (ii) high porosity, (iii) small pore size, and (iv) high thermal stability that enables a high heat-treatment temperature for achieving enhanced Li^+ conductivities of solution-processable SEs ($Li_6PS_5[Cl,Br]$) while being free from any safety concerns under abusive conditions. This is in contrast to those conventional polymers that have restricted thermal stability, including PEO (melting point of ~65 °C).[33,36] An electrospinning process of PI having

https://dx.doi.org/10.1021/acsenergylett.0c00251
ACS Energy Lett. 2020, 5, 718−727

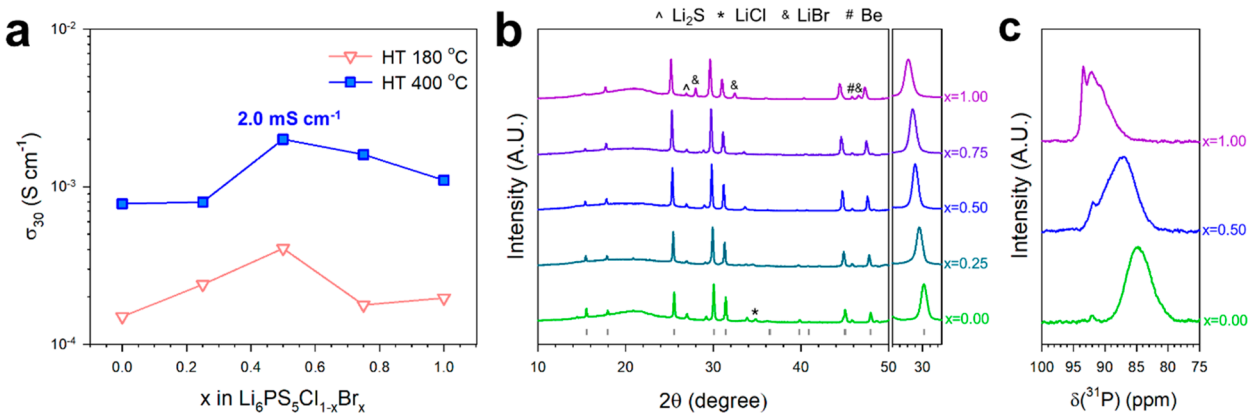

Figure 2. Characterization of solution-processed $Li_6PS_5Cl_{1-x}Br_x$. (a) Li^+ conductivities at 30 °C for solution-processed $Li_6PS_5Cl_{1-x}Br_x$ heat-treated at 180 and 400 °C. (b) Powder XRD patterns and (c) ^{31}P MAS NMR spectra for solution-processed $Li_6PS_5Cl_{1-x}Br_x$ heat-treated at 400 °C. The Bragg positions for argyrodite Li_6PS_5Cl are shown in panel b.

ultrahigh thermal stability (≲500 °C) with inherent fire retardancy was thus developed in this study.

The electrospinning of PI was conducted using polyamic acid precursor solutions, followed by imidization (Figure S1). The imide group for PI was identified by Fourier transform infrared spectroscopy (FTIR). The absorption bands for asymmetric C═O stretching at 1775 cm^{-1}, symmetric C═O stretching at 1720 cm^{-1}, and C−N stretching at 1375 m^{-1} were confirmed (Figure S2).[50] Moreover, the absorption band for N−H stretching in the range of 3300−3500 cm^{-1} was not observed, confirming the complete conversion of polyamic acid into PI by thermal imidization.[51] The electrospinning process renders highly porous interconnected fibrous structures, which is suitable for the uptake of a sufficient amount of liquefied Li_6PS_5[Cl,Br]. Due to the high affinity of EtOH for the polar imide group in PI, the homogeneous Li_6PS_5[Cl,Br]/EtOH solution infiltrates readily into the as-electrospun porous polymeric NWs by simple dropping. The subsequent evaporation of the solvents under vacuum induces crystallization of the original Li_6PS_5[Cl,Br], and further heat treatment at an elevated temperature of ≳180 °C enhances crystallinity.[41,52] After densification by cold pressing under 550 MPa, the final Li_6PS_5[Cl,Br]-infiltrated PI membranes were obtained. The thickness of the resulting PI−Li_6PS_5[Cl,Br] membranes could be controlled by adjusting the thickness of polymeric NWs and/or the amount of SE solution. The fraction of PI in PI−Li_6PS_5[Cl,Br] was 3.6−6.6 wt %. Poly(ether imide) (PEI) showing thermal stability considerably inferior to that of PI was also selected for the electrospun NW as a counter reference.

In our previous works on SE coating and the infiltration of conventional LIB electrodes using solution-processable SEs, heat-treatment temperatures were limited to ≲200 °C.[41,45,46,53] This was due to concerns about any reactions between SEs and electrode active materials and the thermal degradation of the polymeric binder polyvinylidene fluoride (PVDF) (where the latter is the case for only SE-infiltrated electrodes).[41,45,46,48,54] However, a heat-treatment temperature of 200 °C is insufficiently high to obtain high crystallinity, which is required to achieve the correspondingly high Li^+ conductivity of >10^{-3} S cm^{-1}.[41,55,56] In the work presented here, reactivity between SEs and polymers (PI) at elevated temperatures may not be severe, and PI widens the available heat-treatment temperature to 400 °C. This allows us to enhance Li^+ conductivities of solution-processable SEs. Moreover, results of recent investigations of the effects of halides in Li_6PS_5X (X = Cl, Br, or I) on Li^+ dynamics led us to optimization of solution-processable Li argyrodites, $Li_6PS_5Cl_{1-x}Br_x$, with variations in x ($0 \le x \le 1$) heat-treated at 400 °C.[52,57,58]

Li^+ conductivities and their corresponding activation energies for the solution-processed $Li_6PS_5Cl_{1-x}Br_x$ heat-treated at 180 or 400 °C as a function of x were measured by an AC method using Ti/SE/Ti symmetric cells at 30 °C (Figure 2a and Figure S3). The solution-processed single-halogen Li_6PS_5X [Li_6PS_5Cl (x = 0.0) or Li_6PS_5Br (x = 1.0)] exhibited Li^+ conductivities in the range of 0.1−0.2 mS cm^{-1} when heat-treated at 180 °C. The use of multihalogens, that is, $Li_6PS_5Cl_{0.5}Br_{0.5}$, resulted in increased Li^+ conductivities of ≲0.4 mS cm^{-1}. However, the Li^+ conductivities on the order of 10^{-4} S cm^{-1} for the infiltrating sulfide SEs were too low for their application to polymer−SE hybrids because the presence of an insulating polymeric component would reduce Li^+ conductivity by approximately 1 order of magnitude, which translates into conductivities of ≲10^{-5} S cm^{-1} for the resulting films.[27] Importantly, increasing the heat-treatment temperature to 400 °C results in a significant enhancement of Li^+ conductivities, which can be attributed to improved crystallinity and the elimination of organic impurities.[41,52] The highest Li^+ conductivity of 2.0 mS cm^{-1} was achieved for multihalogen composition, that is, $Li_6PS_5Cl_{0.5}Br_{0.5}$. This result is in line with previous results for samples prepared by conventional methods.[57,58] The optimal Li^+ conductivity achieved for $Li_6PS_5Cl_{0.5}Br_{0.5}$ could be explained by the interplay among several factors, including the lattice size, the anion framework polarizability, and the X^-/S^{2-} site disorder, which alter the prefactor and the activation barrier for Li^+ transport.[57] Figure 2b shows the powder X-ray diffraction (XRD) patterns of solution-processed $Li_6PS_5Cl_{1-x}Br_x$ ($0 \le x \le 1$) heat-treated at 400 °C. All samples show the main peaks corresponding to the cubic argyrodite phase (CIF no. 418490 for Li_6PS_5Cl) and marginal impurity peaks for LiX and Li_2S. Along with the substitution of Cl^- with Br^-, the main peaks are shifted to a smaller angle, indicating enlarged lattices due to the ionic size of Br^- [1.82 Å for a coordination number (CN) of 6] being larger than that of Cl^- (1.67 Å for a CN of 6), as shown in the overall increased unit cell volume (Figure S4).[57,59,60] Moreover, ^{31}P magic-angle spinning (MAS) nuclear magnetic resonance (NMR) spectra for solution-processed

https://dx.doi.org/10.1021/acsenergylett.0c00251
ACS Energy Lett. 2020, 5, 718−727

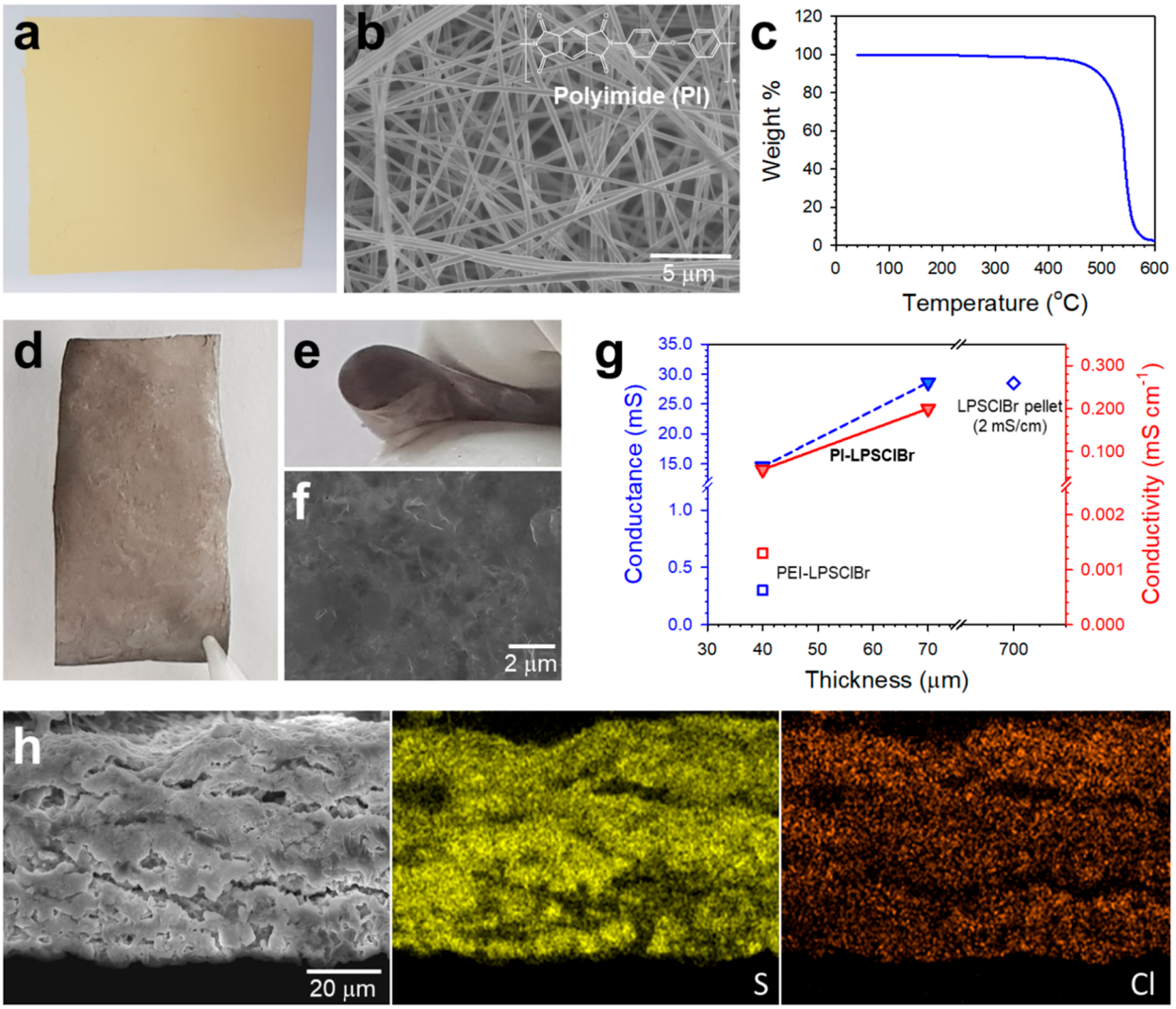

Figure 3. Characterization of electrospun PI NWs and $Li_6PS_5Cl_{1-x}Br_x$-infiltrated PI membranes heat-treated at 400 °C. (a) Photograph and (b) SEM image of an electrospun porous PI NW. The sheet in panel a is 10 cm × 10 cm. (c) TGA profile of electrospun porous PI NWs under a flow of Ar. (d and e) Photographs and (f) surface SEM image of PI−$Li_6PS_5Cl_{0.5}Br_{0.5}$ membranes. (g) Li^+ conductance and conductivities of PI−$Li_6PS_5Cl_{0.5}Br_{0.5}$ membranes as compared with those of PEI−$Li_6PS_5Cl_{0.5}Br_{0.5}$ membranes heat-treated at 180 °C, and conventional $Li_6PS_5Cl_{0.5}Br_{0.5}$ pellets. (h) Cross-sectional SEM image of the PI−$Li_6PS_5Cl_{0.5}Br_{0.5}$ membrane and corresponding EDXS maps of sulfur and chlorine.

$Li_6PS_5Cl_{1-x}Br_x$ heat-treated at 400 °C were obtained (Figure 2c). The overall broadness of the peaks, which could reflect the degree of X^-/S^{2-} site disorder,[61] was the largest for $Li_6PS_5Cl_{0.5}Br_{0.5}$, which correlates well with the Li^+ conductivities (Figure 2a). It is shown that the substitution of Cl^- with Br^- in Li_6PS_5Cl had a negligible effect on the electrochemical oxidative stability from cyclic voltammetry (CV) results (Figure S5).

A photograph and scanning electron microscopy (SEM) image for the electrospun PI membranes are shown in panels a and b of Figure 3, respectively. The SEM image shows that the PI membranes consisted of randomly arranged nanofibers with diameters of ∼500 nm and included a large amount of void spaces. The measured porosity value was in the range of 80−90%, which is high for the uptake of sufficient amounts of SEs. Thermogravimetric analysis (TGA) results under an Ar flow, as shown in Figure 3c, indicate that the onset temperature for thermal decomposition was as high as ∼500 °C. The $Li_6PS_5Cl_{0.5}Br_{0.5}$-infiltrated PI membranes prepared at 400 °C ("PI−LPSClBr" hereafter) are flexible, as shown in the photographs in panels d and e of Figure 3. The bending test result for the PI−LPSClBr using a 3 cm diameter rod also confirms its flexibility (Figure S6 and Movie S1). In addition, their surface SEM image (Figure 3f) shows a compactness without any noticeable cracks. These features are attributed to the resilience of the PI NWs and the deformability of $Li_6PS_5Cl_{0.5}Br_{0.5}$. In contrast, a conventional thin $Li_6PS_5Cl_{0.5}Br_{0.5}$ pellet without using PI (7.5 mg cm^{-2}) resulted in a severe disintegration after cold pressing (Figure S7). It should be emphasized that the excellent mechanical properties of the resulting membranes developed could facilitate their adaptation in industrial production at scale, such as in roll-to-roll processes used for commercial LIB manufacturing.[8,11]

Li^+ conductivities and the conductance of SE membranes as a function of thickness are presented in Figure 3g and Table 1. The Nyquist plots for the SE membranes and the equivalent

https://dx.doi.org/10.1021/acsenergylett.0c00251
ACS Energy Lett. 2020, 5, 718−727

Table 1. Characteristics of Sulfide SE Membranes and Pellets

sample	Li^+ conductance[a] (mS)	thickness (μm)	Li^+ conductivity[a] (mS cm^{-1})	areal mass (mg cm^{-2})
PI–LPSClBr	15	40	0.058	5.0
	29	70	0.20	9.5
PEI–LPSClBr	0.30	40	0.0013	6.3
LPSClBr pellet	29	700	2.0	113

[a]At 30 °C.

circuit model are shown in Figures S8 and S9, respectively. The results of $Li_6PS_5Cl_{0.5}Br_{0.5}$-infiltrated PEI membranes heat-treated at 180 °C ("PEI–LPSClBr" hereafter) are also compared. It is shown that the PEI–LPSCl membranes are also flexible (Figure S10). The PI–LPSClBr membrane shows Li^+ conductivities ranging from 0.058 to 0.20 mS cm^{-1} at 30 °C and varied by thickness (triangles in Figure 3g). These high Li^+ conductivities are attributed to the ability of PI to remain intact at a high heat-treatment temperature of 400 °C at which $Li_6PS_5Cl_{0.5}Br_{0.5}$ can show a conductivity of 2.0 mS cm^{-1} (Figure 2a). In stark contrast, the PEI–LPSClBr heat-treated at 180 °C showed a Li^+ conductivity that was too low (0.0013 mS cm^{-1}, squares in Figure 3g). It is worth noting that Li^+ conductance rather than Li^+ conductivity is more critical for the electrochemical performance of all-solid-state cells. In our previous work, the $LiTiS_2/Li_4Ti_5O_{12}$ ASLB cells that used thin NW–Li_3PS_4 membranes (0.2 mS cm^{-1}, 70 μm) outperformed ASLB that used thick Li_3PS_4 pellets (0.73 mS cm^{-1}, 700 μm).[27] The thin (40–70 μm) PI–LPSClBr showed an ionic conductance (15–29 mS) similar to that of the conventional 700 μm thick $Li_6PS_5Cl_{0.5}Br_{0.5}$ pellet (29 mS, diamond in Figure 3g), suggesting that the use of PI–LPSClBr does not offset the electrochemical performances of ASLBs. Moreover, the low mass loadings of PI–LPSClBr (5.0–9.5 mg cm^{-2} vs ~110 mg cm^{-2} for the conventional thick SE pellet) suggest a significant advantage in the cell-based energy densities of ASLBs. The

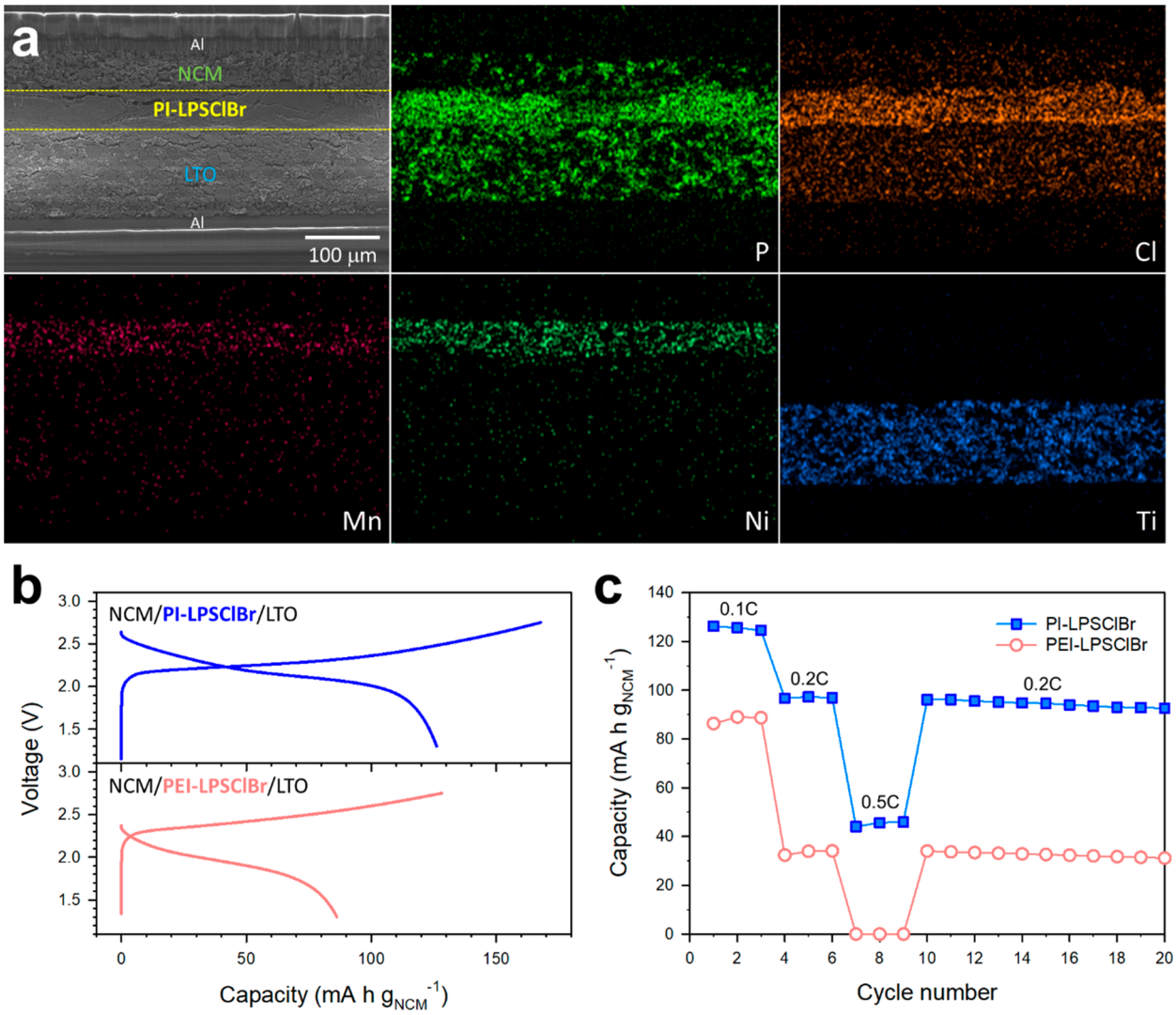

Figure 4. Results of NCM/LTO all-solid-state full cells employing PI (or PEI)–$Li_6PS_5Cl_{0.5}Br_{0.5}$ membranes. (a) Cross-sectional SEM image of NCM/PI–$Li_6PS_5Cl_{0.5}Br_{0.5}$/LTO all-solid-state full cells and corresponding elemental maps, showing a PI–$Li_6PS_5Cl_{0.5}Br_{0.5}$ layer. (b) First-cycle charge–discharge voltage profiles of NCM/PI–$Li_6PS_5Cl_{0.5}Br_{0.5}$/LTO and NCM/PEI–$Li_6PS_5Cl_{0.5}Br_{0.5}$/LTO all-solid-state full cells at 30 °C and (c) their corresponding rate capabilities.

https://dx.doi.org/10.1021/acsenergylett.0c00251
ACS Energy Lett. 2020, 5, 718–727

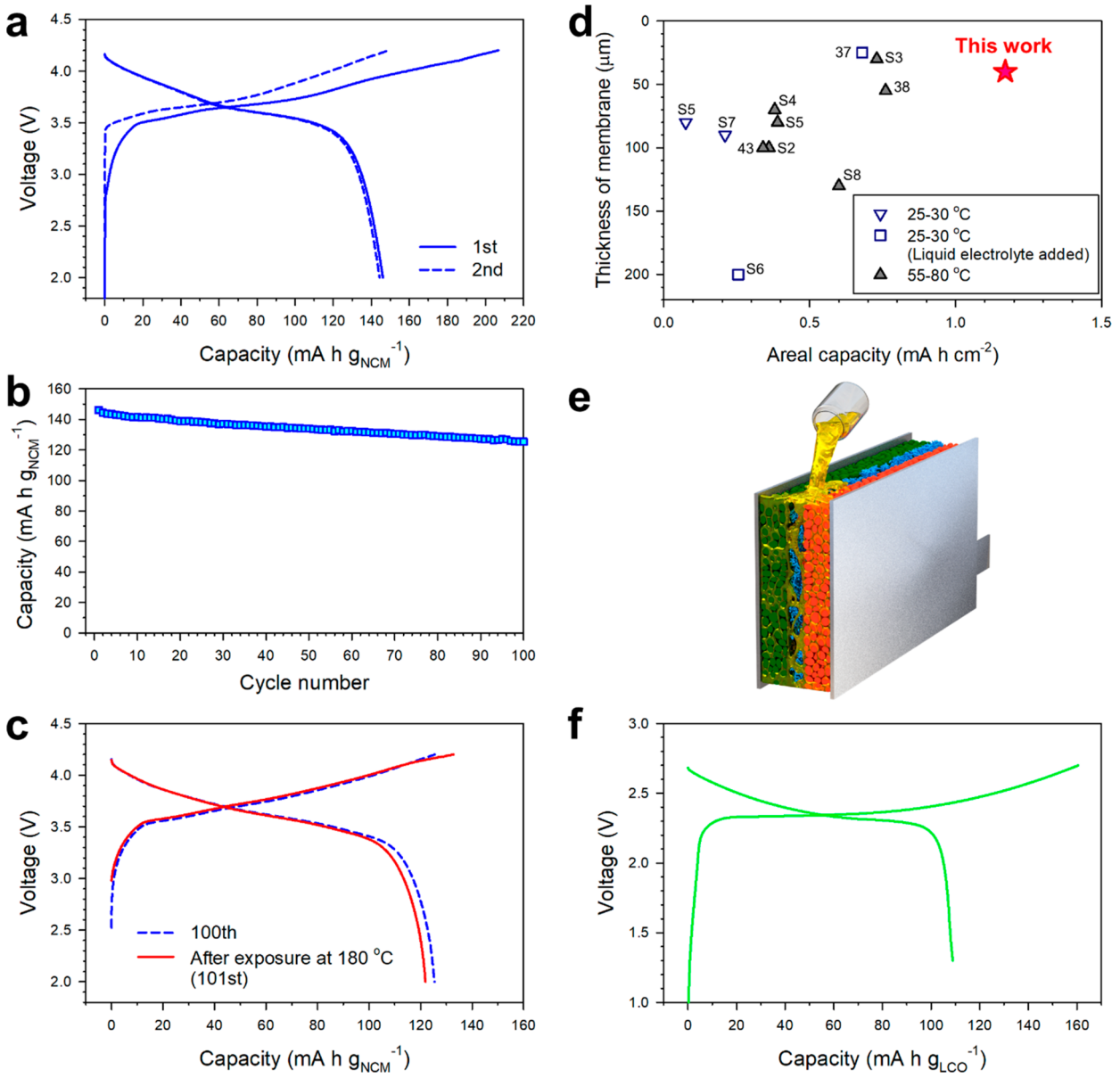

Figure 5. Results of all-solid-state full cells employing PI−$Li_6PS_5Cl_{0.5}Br_{0.5}$ membranes. (a) First two-cycle charge−discharge voltage profiles and (b) corresponding cycling performance of NCM/graphite all-solid-state full cells employing PI−$Li_6PS_5Cl_{0.5}Br_{0.5}$ membranes at 0.1C and 30 °C. (c) Charge−discharge voltage profiles for NCM/graphite all-solid-state full cells employing PI−$Li_6PS_5Cl_{0.5}Br_{0.5}$ membranes at 0.1C and 30 °C before and after exposure to 180 °C for 1 h. (d) Comparison of SE membrane thickness and areal capacity for NCM/graphite all-solid-state full cells employing PI−$Li_6PS_5Cl_{0.5}Br_{0.5}$ membranes with previous results. (e) Schematic illustrating fabrication of ASLBs by injection of liquefied sulfide SEs ($Li_6PS_5Cl_{0.5}Br_{0.5}$/EtOH solution) into Al/LCO/(PI NWs)/LTO/Al assemblies and (f) corresponding first-cycle charge−discharge voltage profiles at 0.05C and 70 °C. The cycling performance corresponding to panel f is shown in Figure S18.

electronic conductivity of the PI−LPSClBr was also measured by the DC polarization method using Ti/PI−LPSClBr/Ti symmetric cells.[58] PI−LPSClBr exhibited an electronic conductivity of ~10^{-9} S cm^{-1} (Figure S11). This value is 5 orders of magnitude lower than the ionic conductivity, which translates into a Li^+ transport number of ~0.99999. Figure 3h shows a cross-sectional SEM image of the PI−LPSClBr and its corresponding energy dispersive X-ray spectroscopy (EDXS) elemental maps for S and Cl. $Li_6PS_5Cl_{0.5}Br_{0.5}$ exists homogeneously across the inner parts of the membranes, which is attributed to the facile penetration of liquefied SEs into the porous PI NWs during the infiltration step and the good mechanical sintering of $Li_6PS_5Cl_{0.5}Br_{0.5}$ upon cold pressing.

For electrochemical characterization, NCM/$Li_4Ti_5O_{12}$ (LTO) all-solid-state full cells employing the 40 μm thick $Li_6PS_5Cl_{0.5}Br_{0.5}$-infiltrated PI or PEI membranes were fabricated. Sheet-type NCM and LTO electrodes prepared by the slurry process were used (details are provided in the Supporting Information). Cross-sectional SEM images for NCM/PI−LPSClBr/LTO ASLBs and the corresponding EDXS elemental maps confirm that thin SE layers are firmly in contact with both the cathode and anode layers without any cracks or short circuits (Figure 4a and Figures S12 and S13). First-cycle charge−discharge profiles at 30 °C for NCM/LTO ASLBs employing PI−LPSClBr and PEI−LPSClBr at 0.22 mA cm^{-2} (~0.1C) and the corresponding rate capabilities are compared in panels b and c of Figure 4. The ASLB employing

https://dx.doi.org/10.1021/acsenergylett.0c00251
ACS Energy Lett. 2020, 5, 718−727

PI−LPSClBr showed a discharge capacity (126 mA h g_{NCM}^{-1}) much higher than that of ASLB employing PEI−LPSClBr (~86 mA g_{NCM}^{-1}). The trend in rate capability was also consistent. This huge difference is attributed to the superior Li^+ conductivity of PI−LPSClBr versus PEI−LPSClBr, thus revealing the rational design that takes advantage of the ultrahigh thermal stability of PI. Moreover, the electrochemical impedance spectroscopy (EIS) measurements for NCM/PI−LPSClBr/LTO ASLBs were performed in discharged states at 2.17 V after the second and 20th cycles, and the corresponding Nyquist plots are displayed in Figure S14. After cycling, the sum of the resistances for NCM/PI−LPSClBr/LTO ASLBs remained constant, indicating that the SE layers remain in good contact with the electrode layers. However, the ASLB using PI−LPSClBr showed a reversible capacity (126 mA h g_{NCM}^{-1}) lower than that of ASLB using a conventional LPSClBr pellet (141 mA h g_{NCM}^{-1}), despite an insignificant difference in conductance between PI−LPSClBr (15 mS) and the LPSClBr pellet (29 mS) (Figure S15). This result could be rooted in the Li^+ insulating property of PI domains that obstruct local ionic contacts at the electrode−SE interfaces.[27] In this regard, development of Li^+ conducting NWs could further improve the electrochemical performance, which will be the subject of our future work.

To demonstrate more practical ASLBs, all-solid-state NCM/Gr full cells employing 40 μm thick PI−LPSClBr were assembled. Their first two-cycle charge−discharge voltage profiles at 0.22 mA cm^{-2} (~0.1C) and 30 °C are displayed in Figure 5a. Despite the Li^+ conductivity of 0.058 mS cm^{-1} for the 40 μm thick PI−LPSClBr, the NCM/Gr ASLBs exhibited a high reversible capacity of 146 mA h g_{NCM}^{-1}, which is comparable to that of ASLBs that employ conventional thick SE layers with a high Li^+ conductivity of >1.0 mS cm^{-1}.[20] This result reveals the importance of ionic conductance rather than ionic conductivity in testing and evaluating the electrochemical performances of ASLBs, something that has been overlooked in research on ASLBs. The energy density of NCM/PI−LPSClBr/Gr ASLBs is 110 Wh kg_{cell}^{-1} based on the weights of cathodes, anodes, SE membranes, and current collectors (156 Wh kg^{-1} excluding the weights of current collectors). This value is much higher than those from previous results using conventional thick SE layers.[24,62] NCM/PI−LPSClBr/Gr ASLBs show a stable cycling performance, retaining 86% of their initial capacity after 100 cycles (Figure 5b). Furthermore, NCM/PI−LPSClBr/Gr ASLBs were subjected to the abuse condition of exposure at a high temperature of 180 °C for 1 h. Under this harsh condition, conventional polymer electrolytes are melted and the resulting all-solid-state cells cannot function properly and may suffer from safety issues.[29,31,34,36] For the purpose of comparison, we also prepared PEO−Li bis(trifluoromethanesulfonyl)imide (LiTFSI) containing 10 wt % Al_2O_3 nanoparticles as a model for the conventional polymer electrolyte or OPC SE. The PEO−LiTFSI−Al_2O_3 films showed considerable thermal shrinkage when exposed to a temperature of 180 °C and lost their original shape completely when exposed to a temperature of 400 °C (Figure S16). By contrast, the charge−discharge voltage profiles for the NCM/PI−LPSClBr/Gr ASLBs after exposure to a temperature of 180 °C still nearly overlapped with those prior to the exposure (Figure 5c), manifesting excellent thermal stability and safety.

The electrochemical performances of NCM/PI−LPSClBr/Gr ASLBs were compared with those when using free-standing SE membranes in terms of the thickness of the membranes and areal capacity, as shown in Figure 5d. Detailed information is summarized in Table S1. In most previous studies, ASLBs employing polymer electrolytes or OPC SE membranes were typically tested at elevated temperatures (55−80 °C).[29,30,36] The thickness of PI−LPSClBr (40 μm) ranked at the lowest level. Moreover, on the basis of previous results, ASLBs using PI−LPSClBr outperformed the case in which a conventional polymer electrolyte or OPC SE membranes were used, despite the similar Li^+ conductivities. This fact could be attributed to the single-ion conducting ability.[11,30]

Finally, motivated by the LE injection process for a LIB manufacturing line, we attempted the fabrication of ASLBs by infiltration of the SE solutions into the preassembled cathode/(polymeric NW membrane)/anode (Figure 5e). Slurry-fabricated conventional $LiCoO_2$ (LCO) and LTO electrodes, typically employed in conventional LIBs, were used. The liquefied $Li_6PS_5Cl_{0.5}Br_{0.5}$ infiltrates into the tortuous porous structures of the LCO/PI/LTO assemblies. Removal of the solvent and the subsequent heat treatment, which was followed by cold pressing, enable the $Li_6PS_5Cl_{0.5}Br_{0.5}$ crystals to densely occupy the void spaces, thus rendering favorable Li^+ conduction pathways throughout the whole batteries. Owing to the limited thermal stability of the PVDF binders in the electrodes, the heat-treatment temperature was set to 180 °C.[41] First-cycle charge−discharge voltage profiles for the $Li_6PS_5Cl_{0.5}Br_{0.5}$-infiltrated LCO/PI/LTO ASLBs at 0.05C and 70 °C are displayed in Figure 5f, in which the initial discharge capacity of 109 mA h g_{LCO}^{-1} is shown. The rate capability and cycling performance of $Li_6PS_5Cl_{0.5}Br_{0.5}$-infiltrated LCO/PI/LTO ASLB cells are also shown in Figures S17 and S18, respectively. The $Li_6PS_5Cl_{0.5}Br_{0.5}$-infiltrated LCO/PI/LTO showed a capacity retention of 74.2% at 0.2C with respect to the capacity at 0.05C and exhibited decent cycling performance (capacity retention of 88.1% after 25 cycles at 0.2C).

In summary, thin, flexible, and high-conductance single-ion conducting SE membranes with ultrahigh thermal stability for ASLBs were developed using a rational design of highly conductive solution-processable SEs as well as mechanically compliant and thermally stable porous PI NW scaffolds. The exceptionally high thermal stability and favorable porous structures of PI NWs enabled the adaptation of highly conductive (2.0 mS cm^{-1}) solution-processable $Li_6PS_5Cl_{0.5}Br_{0.5}$ through an infiltration protocol. The NCM/Gr ASLBs using 40 μm thick $Li_6PS_5Cl_{0.5}Br_{0.5}$-infiltrated PI membranes demonstrated promising electrochemical performances at 30 °C (146 mA h g_{NCM}^{-1}) and excellent thermal stability, outperforming ASLBs that use conventional polymer electrolytes or OCP SE membranes. Finally, a proof of concept of the SE injection process for fabricating ASLBs was successfully demonstrated. LCO/PI/LTO ASLBs activated by the infiltration of the liquefied $Li_6PS_5Cl_{0.5}Br_{0.5}$ into the electrodes/separator assemblies and solidification showed promising electrochemical performances. Although the energy and power densities demonstrated in this study are insufficiently high to compete with the state-of-the-art LIB technologies, we believe that our proof-of-concept results shed light on the developmental principle of SEs in terms of practical manufacturing of ASLBs at scale. Suggested future research directions are as follows. First, further enhancement of Li^+ conductivity for solution-processable SEs should be researched by elaborating on the composition and/or synthetic protocols.[45,52,56,58] Second, development of composite electrodes that withstand high-heat-treatment temperature conditions

https://dx.doi.org/10.1021/acsenergylett.0c00251
ACS Energy Lett. 2020, 5, 718−727

(i.e., thermally stable binders, binder-less electrodes, and interfacial engineering to suppress the reaction between electrode active materials and SEs) should be pursued. Third, evaluation and engineering of SE membranes to make them compatible with alternative high-capacity anodes, including Li metal, Si, and Sn, are required.[53,63,64]

■ ASSOCIATED CONTENT

Supporting Information

The Supporting Information is available free of charge at https://pubs.acs.org/doi/10.1021/acsenergylett.0c00251.

Experimental methods, synthetic scheme of PI NWs, FTIR spectrum for PI, activation energy, unit cell volume, and CV results for solution-processed $Li_6PS_5Cl_{1-x}Br_x$ heat-treated at 400 °C, photograph of PI−LPSClBr during a bending test, photograph of the LPSClBr pellet, Nyquist plots of SE membranes and the equivalent circuit model, photographs of PEI and PEI−LPSClBr, result of DC polarization test, cross-sectional SEM images of NCM/PI−LPSClBr/LTO all-solid-state full cells, Nyquist plots for NCM/PI−LPSClBr/LTO all-solid-state cells, voltage profiles of NCM/PI−LPSClBr/LTO and NCM/(LPSClBr pellet)/LTO all-solid-state full cells, high-temperature exposure test for the OPC SE membrane, and rate capability of LPSClBr-infiltrated LCO/(PI NWs)/LTO ASLB full cells (PDF)

Movie clip of PI−LPSClBr during a bending test (MP4)

■ AUTHOR INFORMATION

Corresponding Authors

Sang-Young Lee − *School of Energy and Chemical Engineering, Ulsan National Institute of Science and Technology (UNIST), Ulsan 44919, South Korea;* orcid.org/0000-0001-7153-0517; Email: syleek@unist.ac.kr

Yoon Seok Jung − *Department of Energy Engineering, Hanyang University, Seoul 04763, South Korea;* orcid.org/0000-0003-0357-9508; Email: yoonsjung@hanyang.ac.kr

Authors

Dong Hyeon Kim − *Department of Energy Engineering, Hanyang University, Seoul 04763, South Korea; School of Energy and Chemical Engineering, Ulsan National Institute of Science and Technology (UNIST), Ulsan 44919, South Korea*

Yong-Hyeok Lee − *School of Energy and Chemical Engineering, Ulsan National Institute of Science and Technology (UNIST), Ulsan 44919, South Korea*

Yong Bae Song − *Department of Energy Engineering, Hanyang University, Seoul 04763, South Korea*

Hiram Kwak − *Department of Energy Engineering, Hanyang University, Seoul 04763, South Korea*

Complete contact information is available at: https://pubs.acs.org/10.1021/acsenergylett.0c00251

Author Contributions

⊥D.H.K. and Y.-H. L. contributed equally to this work.

Notes

The authors declare no competing financial interest.

■ ACKNOWLEDGMENTS

This work was supported by the Technology Development Program to Solve Climate Changes and by the Basic Science Research Program through the National Research Foundation of Korea (NRF) funded by the Ministry of Science, ICT & Future Planning (NRF2017M1A2A2044501, 2018R1A2A1A05019733, and NRF-2018R1A2B6004996).

■ REFERENCES

(1) Goodenough, J. B.; Kim, Y. Challenges for Rechargeable Li Batteries. *Chem. Mater.* **2010**, *22*, 587−603.

(2) Nayak, P. K.; Erickson, E. M.; Schipper, F.; Penki, T. R.; Munichandraiah, N.; Adelhelm, P.; Sclar, H.; Amalraj, F.; Markovsky, B.; Aurbach, D. Review on Challenges and Recent Advances in the Electrochemical Performance of High Capacity Li- and Mn-Rich Cathode Materials for Li-Ion Batteries. *Adv. Energy Mater.* **2018**, *8*, 1702397.

(3) Xu, K. Electrolytes and Interphases in Li-Ion Batteries and Beyond. *Chem. Rev.* **2014**, *114*, 11503−11618.

(4) Hess, S.; Wohlfahrt-Mehrens, M.; Wachtler, M. Flammability of Li-Ion Battery Electrolytes: Flash Point and Self-Extinguishing Time Measurements. *J. Electrochem. Soc.* **2015**, *162*, A3084−A3097.

(5) Rodrigues, M.-T. F.; Babu, G.; Gullapalli, H.; Kalaga, K.; Sayed, F. N.; Kato, K.; Joyner, J.; Ajayan, P. M. A materials perspective on Li-ion batteries at extreme temperatures. *Nat. Energy* **2017**, *2*, 17108.

(6) Feng, X.; Ouyang, M.; Liu, X.; Lu, L.; Xia, Y.; He, X. Thermal runaway mechanism of lithium ion battery for electric vehicles: A review. *Energy Storage Mater.* **2018**, *10*, 246−267.

(7) Jung, Y. S.; Oh, D. Y.; Nam, Y. J.; Park, K. H. Issues and Challenges for Bulk-Type All-Solid-State Rechargeable Lithium Batteries using Sulfide Solid Electrolytes. *Isr. J. Chem.* **2015**, *55*, 472−485.

(8) Hu, Y.-S. Batteries: Getting solid. *Nat. Energy* **2016**, *1*, 16042.

(9) Janek, J.; Zeier, W. G. A solid future for battery development. *Nat. Energy* **2016**, *1*, 16141.

(10) Kato, Y.; Hori, S.; Saito, T.; Suzuki, K.; Hirayama, M.; Mitsui, A.; Yonemura, M.; Iba, H.; Kanno, R. High-power all-solid-state batteries using sulfide superionic conductors. *Nat. Energy* **2016**, *1*, 16030.

(11) Park, K. H.; Bai, Q.; Kim, D. H.; Oh, D. Y.; Zhu, Y.; Mo, Y.; Jung, Y. S. Design Strategies, Practical Considerations, and New Solution Processes of Sulfide Solid Electrolytes for All-Solid-State Batteries. *Adv. Energy Mater.* **2018**, *8*, 1800035.

(12) Zhang, Z.; Shao, Y.; Lotsch, B.; Hu, Y.-S.; Li, H.; Janek, J.; Nazar, L. F.; Nan, C.-W.; Maier, J.; Armand, M.; Chen, L. New horizons for inorganic solid state ion conductors. *Energy Environ. Sci.* **2018**, *11*, 1945−1976.

(13) Miura, A.; Rosero-Navarro, N. C.; Sakuda, A.; Tadanaga, K.; Phuc, N. H. H.; Matsuda, A.; Machida, N.; Hayashi, A.; Tatsumisago, M. Liquid-phase syntheses of sulfide electrolytes for all-solid-state lithium battery. *Nat. Rev. Chem.* **2019**, *3*, 189−198.

(14) Kamaya, N.; Homma, K.; Yamakawa, Y.; Hirayama, M.; Kanno, R.; Yonemura, M.; Kamiyama, T.; Kato, Y.; Hama, S.; Kawamoto, K.; Mitsui, A. A lithium superionic conductor. *Nat. Mater.* **2011**, *10*, 682−686.

(15) Seino, Y.; Ota, T.; Takada, K.; Hayashi, A.; Tatsumisago, M. A sulphide lithium super ion conductor is superior to liquid ion conductors for use in rechargeable batteries. *Energy Environ. Sci.* **2014**, *7*, 627−631.

(16) Kraft, M. A.; Ohno, S.; Zinkevich, T.; Koerver, R.; Culver, S. P.; Fuchs, T.; Senyshyn, A.; Indris, S.; Morgan, B. J.; Zeier, W. G. Inducing High Ionic Conductivity in the Lithium Superionic Argyrodites $Li_{6+x}P_{1-x}Ge_xS_5I$ for All-Solid-State Batteries. *J. Am. Chem. Soc.* **2018**, *140*, 16330−16339.

(17) Adeli, P.; Bazak, J. D.; Park, K. H.; Kochetkov, I.; Huq, A.; Goward, G. R.; Nazar, L. F. Boosting Solid-State Diffusivity and Conductivity in Lithium Superionic Argyrodites by Halide Substitution. *Angew. Chem., Int. Ed.* **2019**, *58*, 8681−8686.

(18) Placke, T.; Kloepsch, R.; Dühnen, S.; Winter, M. Lithium ion, lithium metal, and alternative rechargeable battery technologies: the odyssey for high energy density. *J. Solid State Electrochem.* **2017**, *21*, 1939−1964.

(19) Manthiram, A.; Yu, X.; Wang, S. Lithium battery chemistries enabled by solid-state electrolytes. *Nat. Rev. Mater.* **2017**, *2*, 16103.
(20) Oh, D. Y.; Kim, D. H.; Jung, S. H.; Han, J.-G.; Choi, N.-S.; Jung, Y. S. Single-step wet-chemical fabrication of sheet-type electrodes from solid-electrolyte precursors for all-solid-state lithium-ion batteries. *J. Mater. Chem. A* **2017**, *5*, 20771−20779.
(21) Sakuda, A.; Kuratani, K.; Yamamoto, M.; Takahashi, M.; Takeuchi, T.; Kobayashi, H. All-Solid-State Battery Electrode Sheets Prepared by a Slurry Coating Process. *J. Electrochem. Soc.* **2017**, *164*, A2474−A2478.
(22) Lee, K.; Lee, J.; Choi, S.; Char, K.; Choi, J. W. Thiol−Ene Click Reaction for Fine Polarity Tuning of Polymeric Binders in Solution-Processed All-Solid-State Batteries. *ACS Energy Lett.* **2019**, *4*, 94−101.
(23) Nam, Y. J.; Oh, D. Y.; Jung, S. H.; Jung, Y. S. Toward practical all-solid-state lithium-ion batteries with high energy density and safety: Comparative study for electrodes fabricated by dry- and slurry-mixing processes. *J. Power Sources* **2018**, *375*, 93−101.
(24) Oh, D. Y.; Nam, Y. J.; Park, K. H.; Jung, S. H.; Kim, K. T.; Ha, A. R.; Jung, Y. S. Slurry-Fabricable Li^+-Conductive Polymeric Binders for Practical All-Solid-State Lithium-Ion Batteries Enabled by Solvate Ionic Liquids. *Adv. Energy Mater.* **2019**, *9*, 1802927.
(25) Zhang, J.; Zhong, H.; Zheng, C.; Xia, Y.; Liang, C.; Huang, H.; Gan, Y.; Tao, X.; Zhang, W. All-solid-state batteries with slurry coated $LiNi_{0.8}Co_{0.1}Mn_{0.1}O_2$ composite cathode and Li_6PS_5Cl electrolyte: Effect of binder content. *J. Power Sources* **2018**, *391*, 73−79.
(26) Whiteley, J. M.; Taynton, P.; Zhang, W.; Lee, S. H. Ultra-thin Solid-State Li-Ion Electrolyte Membrane Facilitated by a Self-Healing Polymer Matrix. *Adv. Mater.* **2015**, *27*, 6922−6927.
(27) Nam, Y. J.; Cho, S. J.; Oh, D. Y.; Lim, J. M.; Kim, S. Y.; Song, J. H.; Lee, Y. G.; Lee, S. Y.; Jung, Y. S. Bendable and Thin Sulfide Solid Electrolyte Film: a New Electrolyte Opportunity for Free-Standing and Stackable High-Energy All-Solid-State Lithium-Ion Batteries. *Nano Lett.* **2015**, *15*, 3317−3323.
(28) Ito, S.; Fujiki, S.; Yamada, T.; Aihara, Y.; Park, Y.; Kim, T. Y.; Baek, S.-W.; Lee, J.-M.; Doo, S.; Machida, N. A rocking chair type all-solid-state lithium ion battery adopting Li_2O−ZrO_2 coated $LiNi_{0.8}Co_{0.15}Al_{0.05}O_2$ and a sulfide based electrolyte. *J. Power Sources* **2014**, *248*, 943−950.
(29) Keller, M.; Varzi, A.; Passerini, S. Hybrid electrolytes for lithium metal batteries. *J. Power Sources* **2018**, *392*, 206−225.
(30) Wan, J.; Xie, J.; Mackanic, D. G.; Burke, W.; Bao, Z.; Cui, Y. Status, promises, and challenges of nanocomposite solid-state electrolytes for safe and high performance lithium batteries. *Mater. Today Nano* **2018**, *4*, 1−16.
(31) Liang, J.; Luo, J.; Sun, Q.; Yang, X.; Li, R.; Sun, X. Recent progress on solid-state hybrid electrolytes for solid-state lithium batteries. *Energy Storage Mater.* **2019**, *21*, 308−334.
(32) Liu, W.; Liu, N.; Sun, J.; Hsu, P. C.; Li, Y.; Lee, H. W.; Cui, Y. Ionic Conductivity Enhancement of Polymer Electrolytes with Ceramic Nanowire Fillers. *Nano Lett.* **2015**, *15*, 2740−2745.
(33) Fu, K. K.; Gong, Y.; Dai, J.; Gong, A.; Han, X.; Yao, Y.; Wang, C.; Wang, Y.; Chen, Y.; Yan, C.; Li, Y.; Wachsman, E. D.; Hu, L. Flexible, solid-state, ion-conducting membrane with 3D garnet nanofiber networks for lithium batteries. *Proc. Natl. Acad. Sci. U. S. A.* **2016**, *113*, 7094−7099.
(34) Zhai, H.; Xu, P.; Ning, M.; Cheng, Q.; Mandal, J.; Yang, Y. A Flexible Solid Composite Electrolyte with Vertically Aligned and Connected Ion-Conducting Nanoparticles for Lithium Batteries. *Nano Lett.* **2017**, *17*, 3182−3187.
(35) Liu, W.; Lee, S. W.; Lin, D.; Shi, F.; Wang, S.; Sendek, A. D.; Cui, Y. Enhancing ionic conductivity in composite polymer electrolytes with well-aligned ceramic nanowires. *Nat. Energy* **2017**, *2*, 17035.
(36) Sheng, O.; Jin, C.; Luo, J.; Yuan, H.; Huang, H.; Gan, Y.; Zhang, J.; Xia, Y.; Liang, C.; Zhang, W.; Tao, X. $Mg_2B_2O_5$ Nanowire Enabled Multifunctional Solid-State Electrolytes with High Ionic Conductivity, Excellent Mechanical Properties, and Flame-Retardant Performance. *Nano Lett.* **2018**, *18*, 3104−3112.
(37) Duan, H.; Fan, M.; Chen, W. P.; Li, J. Y.; Wang, P. F.; Wang, W. P.; Shi, J. L.; Yin, Y. X.; Wan, L. J.; Guo, Y. G. Extended Electrochemical Window of Solid Electrolytes via Heterogeneous Multilayered Structure for High-Voltage Lithium Metal Batteries. *Adv. Mater.* **2019**, *31*, 1807789.
(38) Wang, C.; Wang, T.; Wang, L.; Hu, Z.; Cui, Z.; Li, J.; Dong, S.; Zhou, X.; Cui, G. Differentiated Lithium Salt Design for Multilayered PEO Electrolyte Enables a High-Voltage Solid-State Lithium Metal Battery. *Adv. Sci.* **2019**, *6*, 1901036.
(39) Jung, Y. S.; Cavanagh, A. S.; Gedvilas, L.; Widjonarko, N. E.; Scott, I. D.; Lee, S.-H.; Kim, G.-H.; George, S. M.; Dillon, A. C. Improved Functionality of Lithium-Ion Batteries Enabled by Atomic Layer Deposition on the Porous Microstructure of Polymer Separators and Coating Electrodes. *Adv. Energy Mater.* **2012**, *2*, 1022−1027.
(40) Jiang, W.; Liu, Z.; Kong, Q.; Yao, J.; Zhang, C.; Han, P.; Cui, G. A high temperature operating nanofibrous polyimide separator in Li-ion battery. *Solid State Ionics* **2013**, *232*, 44−48.
(41) Kim, D. H.; Oh, D. Y.; Park, K. H.; Choi, Y. E.; Nam, Y. J.; Lee, H. A.; Lee, S.-M.; Jung, Y. S. Infiltration of solution-processable solid electrolytes into conventional Li-ion-battery electrodes for all-solid-state Li-ion batteries. *Nano Lett.* **2017**, *17*, 3013−3020.
(42) Oh, D. Y.; Nam, Y. J.; Park, K. H.; Jung, S. H.; Cho, S.-J.; Kim, Y. K.; Lee, Y.-G.; Lee, S.-Y.; Jung, Y. S. Excellent Compatibility of Solvate Ionic Liquids with Sulfide Solid Electrolytes: Toward Favorable Ionic Contacts in Bulk-Type All-Solid-State Lithium-Ion Batteries. *Adv. Energy Mater.* **2015**, *5*, 1500865.
(43) Pang, Q.; Zhou, L.; Nazar, L. F. Elastic and Li-ion-percolating hybrid membrane stabilizes Li metal plating. *Proc. Natl. Acad. Sci. U. S. A.* **2018**, *115*, 12389−12394.
(44) Chen, S.; Wang, J.; Zhang, Z.; Wu, L.; Yao, L.; Wei, Z.; Deng, Y.; Xie, D.; Yao, X.; Xu, X. In-situ preparation of poly(ethylene oxide)/Li_3PS_4 hybrid polymer electrolyte with good nanofiller distribution for rechargeable solid-state lithium batteries. *J. Power Sources* **2018**, *387*, 72−80.
(45) Park, K. H.; Oh, D. Y.; Choi, Y. E.; Nam, Y. J.; Han, L.; Kim, J. Y.; Xin, H.; Lin, F.; Oh, S. M.; Jung, Y. S. Solution-Processable Glass LiI-Li_4SnS_4 Superionic Conductors for All-Solid-State Li-Ion Batteries. *Adv. Mater.* **2016**, *28*, 1874−1883.
(46) Banerjee, A.; Park, K. H.; Heo, J. W.; Nam, Y. J.; Moon, C. K.; Oh, S. M.; Hong, S. T.; Jung, Y. S. Na_3SbS_4: A Solution Processable Sodium Superionic Conductor for All-Solid-State Sodium-Ion Batteries. *Angew. Chem., Int. Ed.* **2016**, *55*, 9634−9638.
(47) Choi, Y. E.; Park, K. H.; Kim, D. H.; Oh, D. Y.; Kwak, H. R.; Lee, Y. G.; Jung, Y. S. Coatable Li_4SnS_4 Solid Electrolytes Prepared from Aqueous Solutions for All-Solid-State Lithium-Ion Batteries. *ChemSusChem* **2017**, *10*, 2605−2611.
(48) Kim, T. W.; Park, K. H.; Choi, Y. E.; Lee, J. Y.; Jung, Y. S. Aqueous-solution synthesis of Na_3SbS_4 solid electrolytes for all-solid-state Na-ion batteries. *J. Mater. Chem. A* **2018**, *6*, 840−844.
(49) Duchêne, L.; Kim, D. H.; Song, Y. B.; Jun, S.; Moury, R.; Remhof, A.; Hagemann, H.; Jung, Y. S.; Battaglia, C. Crystallization of closo-borate electrolytes from solution enabling infiltration into slurry-casted porous electrodes for all-solid-state batteries. *Energy Storage Mater.* **2019**, DOI: 10.1016/j.ensm.2019.11.027.
(50) Kim, S.; Jang, K. S.; Choi, H. D.; Choi, S. H.; Kwon, S. J.; Kim, I. D.; Lim, J. A.; Hong, J. M. Porous polyimide membranes prepared by wet phase inversion for use in low dielectric applications. *Int. J. Mol. Sci.* **2013**, *14*, 8698−8707.
(51) Kong, L.; Yan, Y.; Qiu, Z.; Zhou, Z.; Hu, J. Robust fluorinated polyimide nanofibers membrane for high-performance lithium-ion batteries. *J. Membr. Sci.* **2018**, *549*, 321−331.
(52) Yubuchi, S.; Uematsu, M.; Deguchi, M.; Hayashi, A.; Tatsumisago, M. Lithium-Ion-Conducting Argyrodite-Type Li_6PS_5X (X = Cl, Br, I) Solid Electrolytes Prepared by a Liquid-Phase Technique Using Ethanol as a Solvent. *ACS Appl. Energy Mater.* **2018**, *1*, 3622−3629.
(53) Kim, D. H.; Lee, H. A.; Song, Y. B.; Park, J. W.; Lee, S.-M.; Jung, Y. S. Sheet-type Li_6PS_5Cl-infiltrated Si anodes fabricated by

solution process for all-solid-state lithium-ion batteries. *J. Power Sources* **2019**, *426*, 143−150.
(54) Park, K. H.; Kim, D. H.; Kwak, H.; Jung, S. H.; Lee, H.-J.; Banerjee, A.; Lee, J. H.; Jung, Y. S. Solution-Derived Glass-Ceramic $NaI{\cdot}Na_3SbS_4$ Superionic Conductors for All-Solid-State Na-Ion Batteries. *J. Mater. Chem. A* **2018**, *6*, 17192−17200.
(55) Yu, C.; Ganapathy, S.; Hageman, J.; van Eijck, L.; van Eck, E. R. H.; Zhang, L.; Schwietert, T.; Basak, S.; Kelder, E. M.; Wagemaker, M. Facile Synthesis toward the Optimal Structure-Conductivity Characteristics of the Argyrodite Li_6PS_5Cl Solid-State Electrolyte. *ACS Appl. Mater. Interfaces* **2018**, *10*, 33296−33306.
(56) Yubuchi, S.; Uematsu, M.; Hotehama, C.; Sakuda, A.; Hayashi, A.; Tatsumisago, M. An argyrodite sulfide-based superionic conductor synthesized by a liquid-phase technique with tetrahydrofuran and ethanol. *J. Mater. Chem. A* **2019**, *7*, 558−566.
(57) Kraft, M. A.; Culver, S. P.; Calderon, M.; Böcher, F.; Krauskopf, T.; Senyshyn, A.; Dietrich, C.; Zevalkink, A.; Janek, J.; Zeier, W. G. Influence of Lattice Polarizability on the Ionic Conductivity in the Lithium Superionic Argyrodites Li_6PS_5X (X = Cl, Br, I). *J. Am. Chem. Soc.* **2017**, *139*, 10909−10918.
(58) Zhou, L.; Park, K.-H.; Sun, X.; Lalère, F.; Adermann, T.; Hartmann, P.; Nazar, L. F. Solvent-Engineered Design of Argyrodite Li_6PS_5X (X = Cl, Br, I) Solid Electrolytes with High Ionic Conductivity. *ACS Energy Lett.* **2019**, *4*, 265−270.
(59) Huheey, J. E.; Keiter, E. A.; Keiter, R. L. *Inorganic Chemistry: Principles of Structure and Reactivity*, 4th ed.; HarperCollins College Publishers, 1993.
(60) Kwak, H.; Park, K. H.; Han, D.; Nam, K.-W.; Kim, H.; Jung, Y. S. Li^+ conduction in air-stable Sb-Substituted Li_4SnS_4 for all-solid-state Li-Ion batteries. *J. Power Sources* **2020**, *446*, 227338.
(61) Deiseroth, H.-J.; Kong, S.-T.; Eckert, H.; Vannahme, J.; Reiner, C.; Zaiss, T.; Schlosser, M. Li_6PS_5X: A Class of Crystalline Li-Rich Solids With an Unusually High Li^+ Mobility. *Angew. Chem., Int. Ed.* **2008**, *47*, 755−758.
(62) Jung, S. H.; Kim, U.-H.; Kim, J.-H.; Jun, S.; Yoon, C. S.; Jung, Y. S.; Sun, Y.-K. Ni-Rich Layered Cathode Materials with Electro-chemo-Mechanically Compliant Microstructure for All-Solid-State Li Batteries. *Adv. Energy Mater.* **2019**, 1903360.
(63) Whiteley, J. M.; Kim, J. W.; Kang, C. S.; Cho, J. S.; Oh, K. H.; Lee, S. H. Tin Networked Electrode Providing Enhanced Volumetric Capacity and Pressureless Operation for All-Solid-State Li-Ion Batteries. *J. Electrochem. Soc.* **2015**, *162*, A711−A715.
(64) Cheng, X. B.; Zhang, R.; Zhao, C. Z.; Zhang, Q. Toward Safe Lithium Metal Anode in Rechargeable Batteries: A Review. *Chem. Rev.* **2017**, *117*, 10403−10473.

NOTE ADDED AFTER ASAP PUBLICATION

This paper was published ASAP on February 12, 2020, with an incorrect value in Table 1. The corrected version was reposted on February 18, 2020.

https://dx.doi.org/10.1021/acsenergylett.0c00251
ACS Energy Lett. 2020, 5, 718−727